Supporting information

Electrochemical Reconstruction Leading to Borate-linked $[Co(Fe)]_8B_2O_{16}H_2$ Crystalline Phase for Efficient and Stable OER

Xing-Hui Zhang[a], Yi-Fan Hu[a], Zhi-Pan Liu*[ab]

a. Collaborative Innovation Center of Chemistry for Energy Material, Shanghai Key Laboratory of Molecular Catalysis and Innovative Materials, Key Laboratory of Computational Physical Science, Department of Chemistry, Fudan University, Shanghai 200433, China. *E-mail: zpliu@fudan.edu.cn

b. State Key Laboratory of Organometallic Chemistry, Shanghai Institute of Organic Chemistry, Chinese Academy of Sciences, Shanghai 200032, China

Experimental

Materials and Methods

Iron (Ⅲ) Sulfate ($Fe_2(SO_4)_3$, 99%) was obtained from Adamas. Cobalt (Ⅱ) acetate tetrahydrate ($Co(CH_3COO)_2{\cdot}4H_2O$, 99.5%) was obtained from Macklin. Sodium borohydride ($NaBH_4$, 96%), Iron (Ⅲ) nitrate nonahydrate ($Fe(NO_3)_3{\cdot}9H_2O$, 98.5%), Potassium hydroxide (KOH, 85%) were obtained from Sinopharm Chemical Reagent Co., Ltd. All the chemicals were used directly without further purification. All aqueous solutions were prepared using deionized (DI) water with a resistivity of 18.2 MΩ cm.

Characterization

Powder X-ray diffraction (XRD) patterns were obtained on a Bruker D8 with Cu (Kα = 0.15406 nm) as the X-ray source. High-resolution transmission electron microscopy (HR-TEM) data were obtained using an FEI Tecnai G2 F20 S-TWIN transmission electron microscope operating at 200 kV. Elemental mapping was performed on a JEOL-ARM 200F instrument equipped with a Kevex EDX detector (JED 2300T) operating at 200 kV. Fourier transform infrared (FT-IR) spectras were recorded in the range of 4000-1000 cm-1 on a NICOLET iS50 FT-IR spectrometer. Raman wavenumber were recorded using the Horiba Jobin Yvon XploRA micro Raman system with a laser wavelength of 532 nm and a resolution of 4.6 cm-1. The Brunauer-Emmett-Teller (BET) surface area of the products were measured using nitrogen adsorption-desorption (TriStar II 3020). The actual contents of Co, Fe and B were determined by inductively coupled plasma-optical emission spectrometry (ICP-OES, Aglient 5110). All samples were digested with concentrated nitric acid before testing.

Synthesis of catalysts

Synthesis of Co_xFe_y-B: The synthesis methods mentioned above are similar, with the only difference being the addition of cobalt acetate and ferric nitrate in different feed ratios.

Synthesis of Co_4Fe and Co-p: The synthesis methods are similar to that mentioned above, with the only difference being the use of sodium hydroxide instead of sodium borohydride.

Preparation of working electrode

The glassy carbon electrode was polished with Al_2O_3 polishing powder before using, rinsed with deionized water and naturally dried. Then, 4.8 mg of catalyst was dispersed in a mixture consisting of 0.25 mL isopropanol, 0.75 mL deionized water and 0.05 mL Nafion (5% in a mixture of water and alcohol). The suspension was ultrasonicated for 1 h to form a homogeneous ink. After that, 5.24 μL ink was dropped on the glassy carbon electrode and placed in the air to dry naturally.

Electrochemical testing

All electrochemical tests were performed on a Princeton electrochemical workstation using a Hg/HgO as the reference electrode, platinum wire as the counter electrode, a rotating disk electrode with a rotation speed of 2000 rpm as the working electrode, and 1 M KOH as the electrolyte. This scan rate is slow enough to ensure steady-state behavior at the electrode surface, and the rotation rate is sufficiently fast to aid in product removal and limit bubble formation from evolved O_2 at the electrode surface.

Before testing, cyclic voltammetry (CV) measurements were first conducted at a scan rate of 50 mV/s between 0.5-1.7 V vs. RHE. The linear sweep voltammetry (LSV) curves were collected at 5 mV/s between 0.5-1.7

V vs. RHE. The stability was tested at the fixing voltage corresponding to the current density of 10 mA/cm^2. Electrochemical impedance spectroscopy was conducted at 1.51 V vs. RHE from 10000 Hz to 0.01 Hz with an amplitude of 5 mV. The series resistance (Rs) values were determined using electrochemical impedance (EIS) measurement data and later used for ohmic drop compensation. CV was performed in the non-Faradaic region at scan rates of 5, 10, 15, 20 and 25 mV/s, and the third cycle value was taken to calculate ECSA.

Based on Tafel analysis for multi-electron transfer reactions, the Tafel slope can be calculated as the following[1]:

$$b = \frac{\alpha\eta}{\alpha log i_{=}} \frac{2.303RT}{\alpha F}$$

$$\alpha = \frac{nb}{\nu} + n_{r\beta}$$

where n_b is the number of electrons transferred before the PDS, n_r is the number of electrons transferred during the PDS, v is the number of PDS repeated during the reaction.

To quantify the double-layer capacitance, cyclic voltammetry (CV) was performed within a potential range where no significant Faradaic processes occur. This range was identified from static CV measurements and typically corresponds to a 0.1 V potential window centered at the open-circuit potential (OCP) of the system. Within this non-Faradaic region, all measured current is assumed to originate from double-layer charging. The charging current was then obtained from CVs conducted at multiple scan rates.

In Situ Surface Enhanced Raman Spectroscopy.

Raman experiments were performed in a single-compartment, custom-made electrochemical Teflon cell at room temperature. The wavelength of the excitation light source was 532 nm, with a laser power of ~100% with the grading of 2400/mm. Thirty consecutive scans, with 1 s exposure time per scan, produced each spectrum with a resolution of 1.3 cm^{-1}. To ensure high confidence and reproducibility in the quality of the obtained spectra, we calibrated the energy shift using the 520.7 cm^{-1} peak of silicon. We first electrically deposited a layer of gold on the working electrode to obtain the surface-enhanced effect. Using a glassy carbon electrode as the working electrode, silver chloride as the reference electrode, and platinum wire as the counter electrode, electrodeposition was carried out at a -0.5 V vs Ag/AgCl in 5 mg/mL $HAuCl_4$+0.1 M $NaClO_4$ electrolyte for 400 seconds. The Raman signals were recorded in situ at OCP and under different applied potentials spanning from 0.5-1.7 V vs. RHE in 1 M KOH.

Determination of Faraday efficiency

The Faradaic efficiency of O_2 production by each catalyst was measured using a RRDE apparatus. The collection efficiency N of the rotating ring-disk electrode assembly was independently determined to be N = 38% from reducing $K_3Fe(CN)_6$ at a GC electrode and reoxidizing it at the Pt ring. RRDE measurements were conducted in a cell purged for ~30 min with Ar and then blanketed with Ar during the experiment. Before any ring currents were collected, the Pt ring was polished by hand with 1 μm MetaDi Supreme diamond slurry (Buehler) first on a Nylon polishing cloth (Buehler) and then on a Microcloth polishing pad (Buehler), followed by rinsing in pure water. The disk electrode was then held at open circuit for 500 s, and the ring electrode was held at 0.4 V vs RHE in Ar-saturated 1 M KOH. This was to establish the background current at the ring electrode. The magnitude of the background currents was typically $|i_{ring}| < 3$ μA. The disk electrode was then held at 0.5, 1, 2 , 5, and 10 mA/cm^2 at 2000 rpm for 500 s in 1 M KOH, while the ring was held constant at 0.4 V vs RHE.

In this setup, the disk electrode generates oxygen at a constant rotation speed of 2000 rpm under a current density ranging from 0.1 to 10 mA/cm², while the surrounding Pt ring electrode, held at a constant potential of 0.4 V vs. RHE, rapidly reduces O_2 to H_2O_2[2]. Representative disk and ring currents for Co_4Fe-B are shown in Fig. S7a. The Faradaic efficiency was calculated based on the ring current collected during the measurements while the disk electrode was maintained at a constant current density of 1 mA/cm² per geometric area. This current density was chosen to ensure significant O_2 production while minimizing local saturation and bubble formation at the disk electrode. The Faradaic efficiency is directly proportional to the ratio of the ring current to the disk current and can be calculated using the following equation:

$$FE = \frac{2ir}{idN}$$

where i_r is the measured ring current, i_d is the disk current, and N=0.38 represents the collection efficiency of the RRDE.

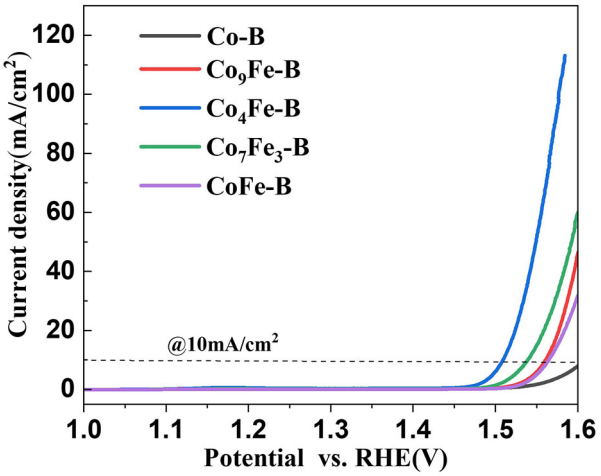

Figure S1. LSV curves (a) of catalysts with different molar ratio of Co:Fe. (b) Cyclic voltammograms of Co_4Fe-B at different scan rates (5-25 mV/s).

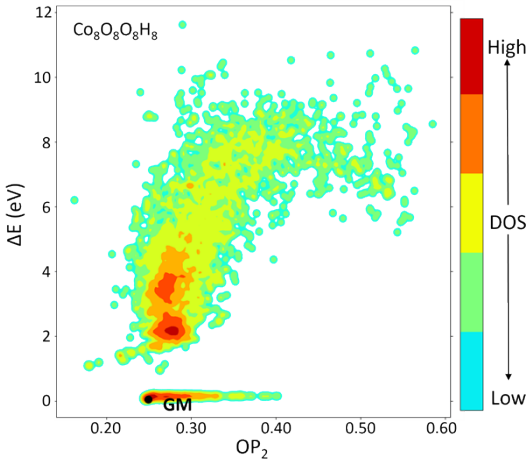

Figure S2. Global PES of CoOOH.

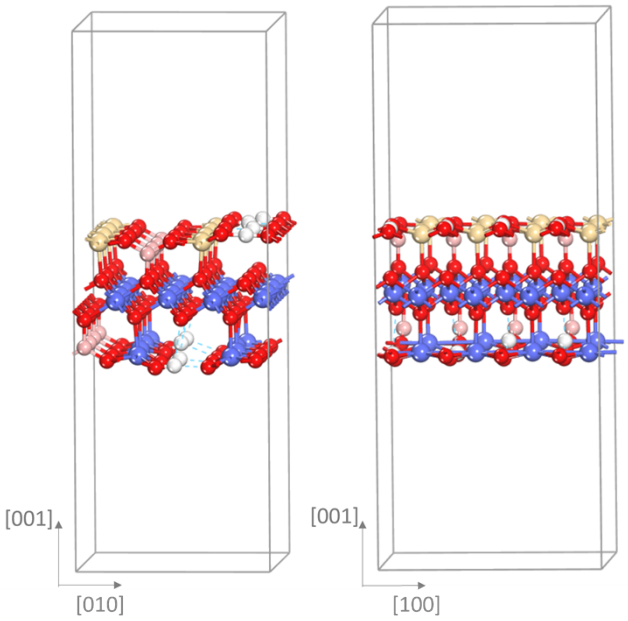

Figure S3. Fe-adopted $Co_8B_2O_{16}H_2$ [110] slab model. Light orange: Fe; blue: Co; red: O; pink: B; white: H.

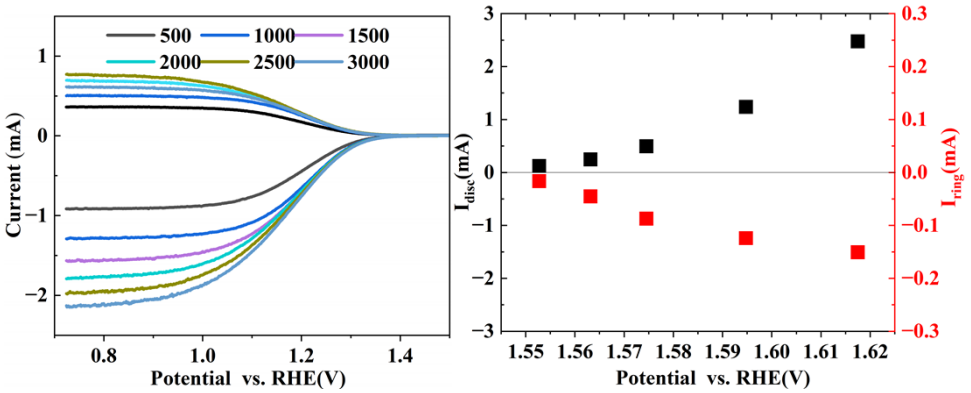

Figure S4. (a) Determination of the ring collection efficiency at different rotation rates. (b) Rotating ring-disc electrode (RRDE) measurement of Co_4Fe-B in 1 M KOH.

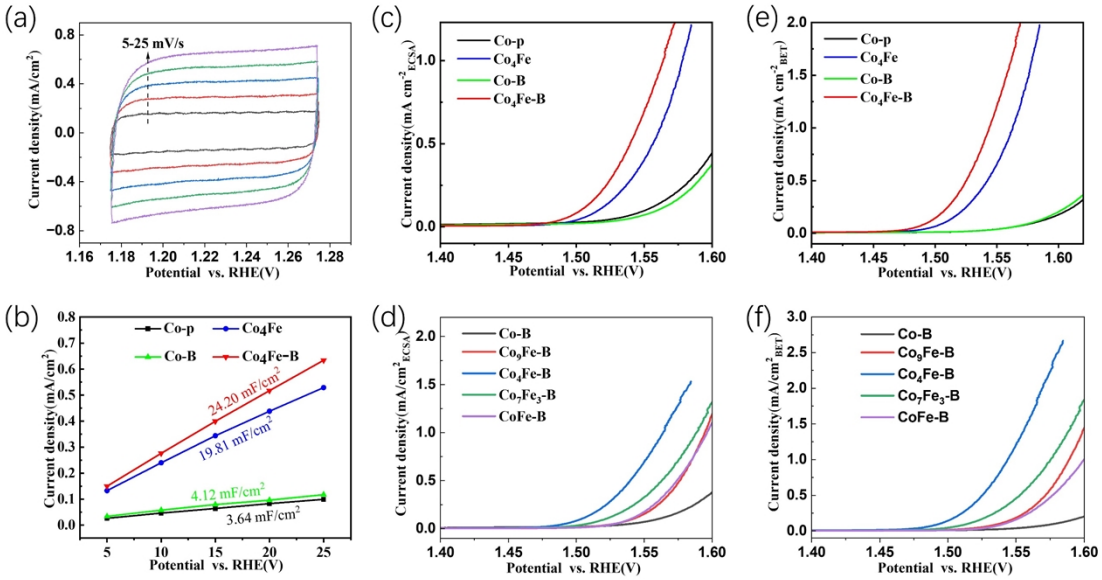

Figure S5. (a) Cyclic voltammograms of Co_4Fe-B at different scan rates (5-25 mV/s). (b) The Corresponding C_{dl} values of Co_xFe_y-B. Stabilized LSV curves of Co_xFe_y-B samples normalized to their (c), (d) ECSA and (e), (f) BET surface areas.

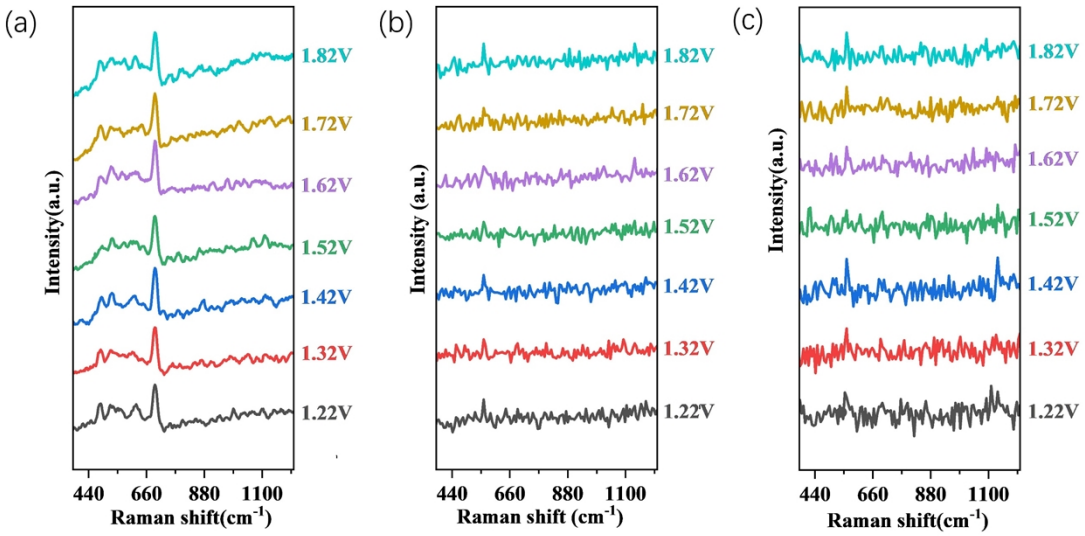

Figure S6. In-situ Raman spectra of (a) Co-B, (b) Co_4Fe and (c) Co-p collected in 0.1 M KOH electrolyte during the multi-potential steps.

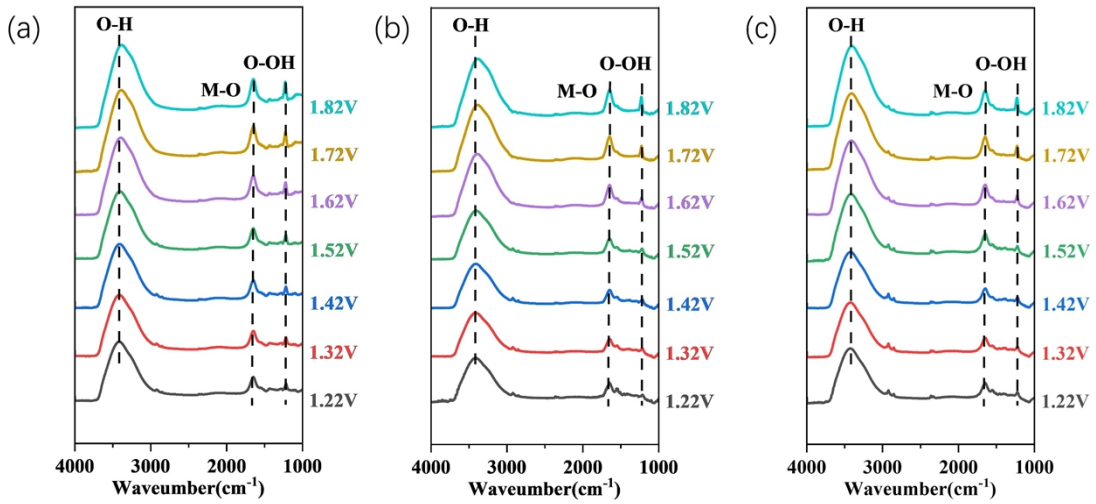

Figure S7. In-situ FT-IR spectra of (a) Co-B, (b) Co_4Fe and (c) Co-p collected in 0.1 M KOH electrolyte during the multi-potential steps.

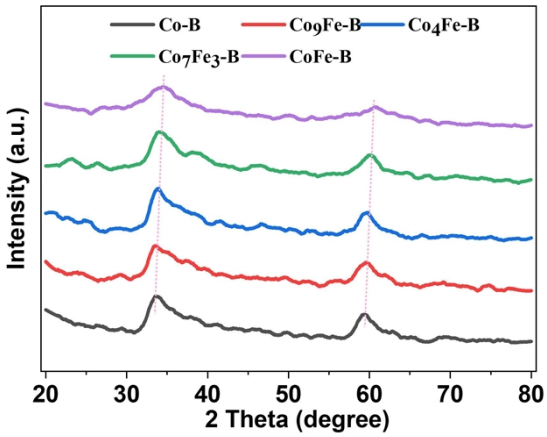

Figure S8. XRD patterns of Co_xFe_y-B catalysts.

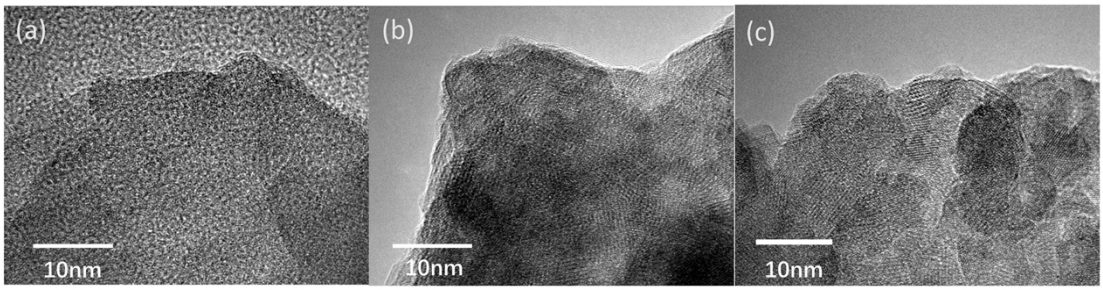

Figure S9. High-resolution TEM images of (a) Co-B, (b) Co_4Fe and (c) Co-p.

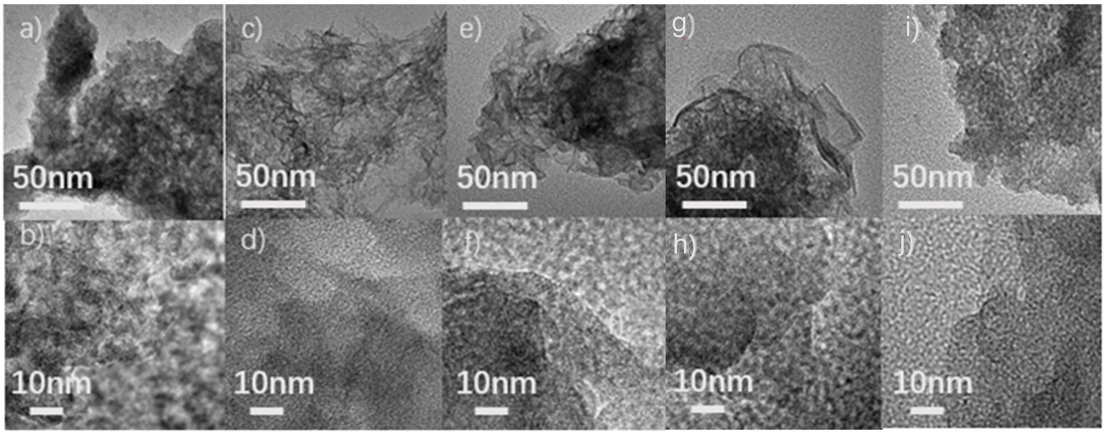

Figure S10. High-resolution TEM images of (a) (b)Co-B, (c) (d) Co_9Fe-B, (e) (f) Co_4Fe-B, (g) (h) Co_7Fe_3-B, (i) (j), CoFe-B.

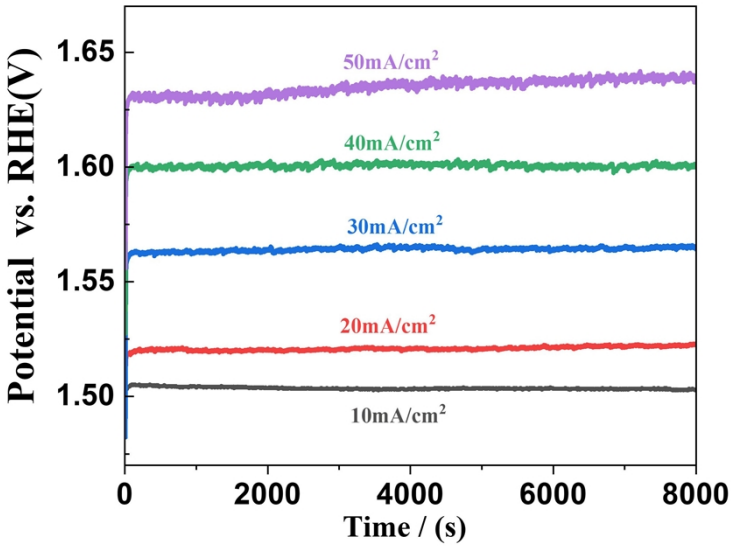

Figure S11. Stability test of Co4Fe-B catalyst at different current densities.

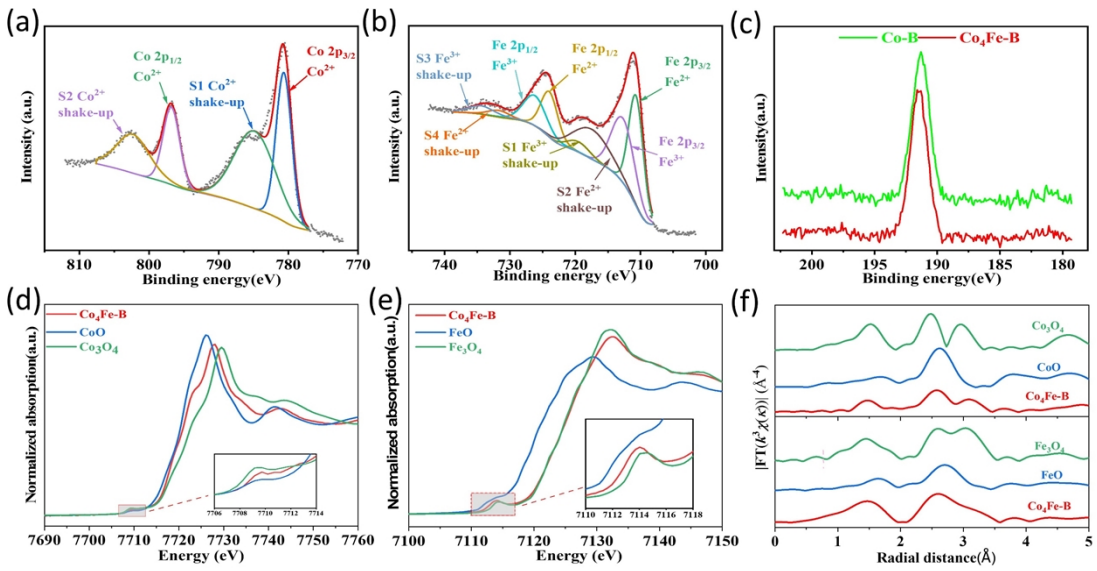

Figure S12. XPS spectra of (a,) Co 2p, (b) Fe 2p and (c) B 1s of Co_4Fe-B. Co (d) and Fe (e) K-edge XANES spectra of Co_4Fe-B. (f) EXAFS spectra of Co_4Fe-B including CoO, Co_3O_4, FeO and Fe_3O_4 as references.

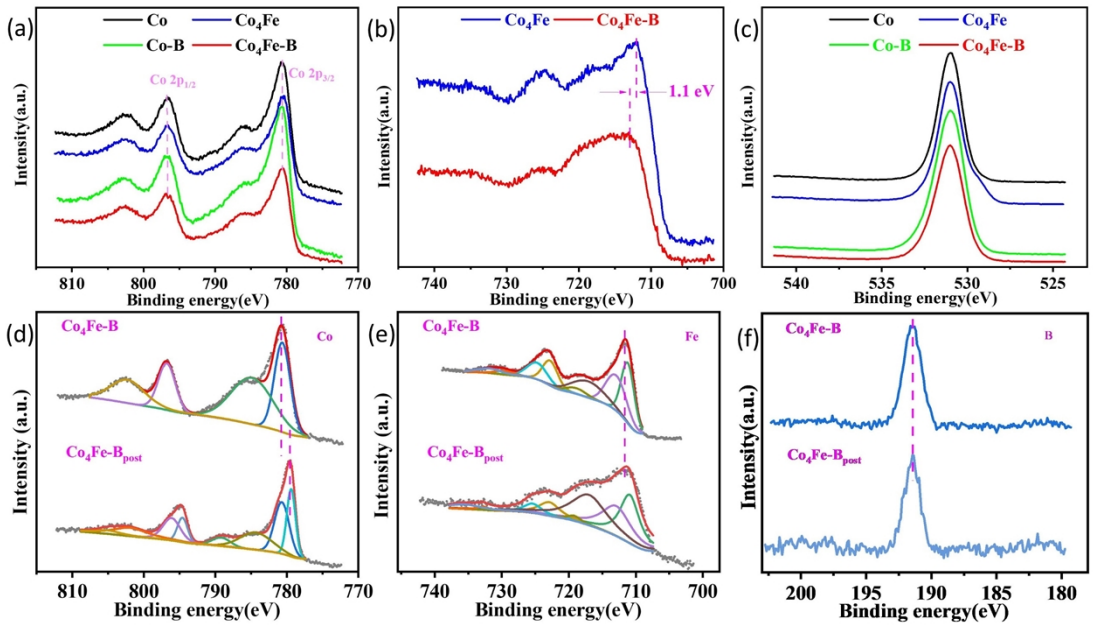

Figure S13. XPS spectra of (a) Co 2p, (b) Fe 2p and (c) O 1s of Co_4Fe-B. XPS spectra of (d) Co 2p, (e) Fe 2p and (f) B 1s of Co_4Fe-B after long-term stability testing.

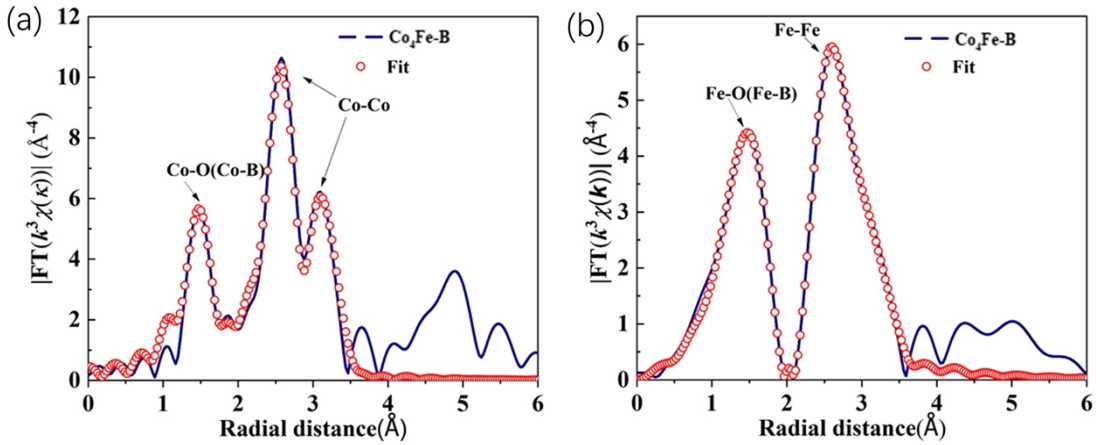

Figure S14. **Co K-edge (a) EXAFS spectra of Co_4Fe-B including Co foil, CoO, Co_3O_4 and $Co(OH)_2$ as references. (c) Fe K-edge EXAFS spectra of Co_4Fe-B including Fe foil, FeO and Fe_3O_4 as references.**

Table S1. Selected Co-based catalyst towards the oxygen evolution reaction.

Catalyst	Electrolyte	η@10mA/cm^2(mV)	Tafel Slope(mV/dec)	Refs.
Co_3O_4	1 M KOH	359	82	[3]
m-P/Co_3O_4	1 M KOH	314	66	[3]
h-P/Co_3O_4	1 M KOH	334	74	[3]
Co_3O_4/CoFe oxide DSNBs	1 M KOH	297	61	[4]
Co/NGC-3	1 M KOH	396	92	[5]
CoO/Co_4N	1 M KOH	398	83	[6]
N-NiCoP$_x$/NCF	1 M KOH	298	60	[7]
$CoSe_2$	1 M KOH	325	80	[8]
CoS_2/G	1 M KOH	300	56	[9]
CoO_x NPs/BNG	1 M KOH	295	57	[10]
Fe-CoOOH/G	1 M KOH	330	37	[11]
Co_2P	1 M KOH	364		[12]
$Co(OH)_2$@NCNTs@NF	1 M KOH	270	72	[13]
$FeCo_3N$	1 M KOH	294	49	[14]
CoFe(OH)$_x$	1 M KOH	294	63	[15]
CoFe alloy/N	1 M KOH	340	78	[16]
CoFe PBA	1 M KOH	305	36	[17]
CoB	1 M KOH	355	49	[18]
CoB/g-C_3N_4	1 M KOH	360	94	[19]
CoB	1 M KOH	290	62	[20]
r-B-$CoFe_2O_4$	1 M KOH	240	32	[21]

Table S2. Structural information of the global PES dataset for G-NN potential training

Species	N_{atm}	cluster	layer	bulk	total	Species	N_{atm}	cluster	layer	bulk	total
Co15	15	0	90	1	91	H6-Co25	31	0	56	0	56
Co27	27	0	52	0	52	H6-Co26	32	0	0	62	62
Co28	28	0	43	1	44	H6-O1-Co24	31	0	144	0	144
Co29	29	0	10	0	10	H6-O11-Co8	25	0	129	328	457
O1	1	2	1	0	3	H6-O12-Co6	24	0	23	164	187
O1-Co16	17	0	12	0	12	H6-O15-Co8	29	0	35	0	35
O2-Co16	18	0	0	17	17	H6-O16-Co9	31	0	17	0	17
O2-Co31	33	0	69	0	69	H6-O21-Co14	41	0	2	0	2
O2-Co32	34	0	25	0	25	H6-B1-O10-Co8	25	0	22	125	147
O4	4	0	15	0	15	H6-B1-O11-Co7	25	0	6	92	98
O5-Co30	35	0	64	0	64	H6-B1-O14-Co8	29	0	10	47	57
O5-Co31	36	0	31	0	31	H6-B2-O9-Co8	25	0	8	53	61
O6-Co8	14	0	2	26	28	H6-B2-O11-Co6	25	0	8	15	23
O7-Co8	15	0	9	99	108	H6-B2-O13-Co8	29	0	2	18	20
O8-Co6	14	238	0	0	238	H6-B2-O15-Co6	29	0	10	25	35
O8-Co8	16	265	7	2742	3014	H6-B3-O8-Co8	25	0	5	28	33
O10-Co8	18	0	18	619	637	H6-B3-O12-Co8	29	0	7	16	23
O11	11	0	78	24	102	H6-B4-O1-Co20	31	0	4	11	15
O11-Co12	23	0	0	1	1	H6-B4-O7-Co8	25	0	3	20	23
O11-Co16	27	0	0	3	3	H6-B6-O5-Co8	25	0	8	16	24
O12-Co8	20	53	16	2322	2391	H7-Co27	34	0	1	34	35
O12-Co12	24	0	0	3	3	H7-O15-Co8	30	0	130	329	459
O13-Co12	25	0	0	5	5	H7-O16-Co8	31	0	47	1	48
O14-Co12	26	0	0	14	14	H7-O17-Co16	40	0	23	0	23
O15-Co12	27	0	0	5	5	H7-B1-O14-Co8	30	0	3	41	44

O15-Co16	31	0	0	6	6	H7-B1-O15-Co7	30	0	2	65	67
O16-Co8	24	0	216	139	355	H7-B2-O13-Co8	30	0	14	54	68
O16-Co12	28	0	0	518	518	H7-B2-O14-Co8	31	0	12	54	66
O17-Co12	29	0	1	0	1	H7-B2-O15-Co6	30	0	14	31	45
O18-Co11	29	0	1	0	1	H7-B3-O12-Co8	30	0	11	73	84
O18-Co12	30	0	0	45	45	H7-B3-O15-Co5	30	0	4	4	8
O20-Co16	36	0	0	11	11	H7-B4-O11-Co8	30	0	12	119	131
O22-Co20	42	0	0	11	11	H7-B5-O10-Co8	30	0	9	46	55
O23-Co20	43	0	0	6	6	H8-O8-Co4	20	0	360	310	670
O24-Co20	44	0	0	2	2	H8-O14-Co8	30	0	27	0	27
O26-Co20	46	0	0	9	9	H8-O15-Co8	31	0	27	0	27
B1-O3-Co1	5	1	0	0	1	H8-O16-Co8	32	0	186	924	1110
B2-O6-Co2	10	0	0	1	1	H8-O17-Co15	40	0	3	0	3
B2-O10-Co6	18	0	0	8	8	H8-O23-Co14	45	0	2	0	2
B4-O8-Co2	14	0	4	6	10	H8-O23-Co15	46	0	19	0	19
B4-O10-Co4	18	0	7	10	17	H8-O23-Co16	47	0	4	2	6
B4-O12-Co4	20	0	42	156	198	H8-O24-Co16	48	0	0	3	3
B4-O12-Co6	22	0	21	225	246	H8-B1-O14-Co7	30	0	14	40	54
B4-O16-Co8	28	0	19	196	215	H8-B1-O16-Co7	32	0	67	532	599
B4-O20-Co12	36	0	7	259	266	H8-B2-O14-Co8	32	0	7	115	122
B4-O24-Co12	40	0	6	75	81	H8-B2-O16-Co6	32	0	7	12	19
B6-O18-Co6	30	0	8	54	62	H8-B4-O48-Co28	88	0	63	86	149

B8-Co16	24	0	0	5	5	H8-B8-O32-Co32	80	0	0	11	11
B8-O16-Co4	28	0	27	387	414	H8-B8-O40-Co32	88	0	2	34	36
B8-O20-Co8	36	0	2	309	311	H8-B12-O36-Co32	88	0	1	15	16
B8-O24-Co8	40	0	172	392	564	H8-B24-O48-Co2	82	0	93	37	130
B8-O32-Co16	56	0	0	2	2	H9-O19-Co8	36	0	140	243	383
B10-Co14	24	0	0	2	2	H9-B1-O18-Co8	36	0	7	26	33
B12-Co12	24	0	0	2	2	H9-B1-O19-Co7	36	0	1	0	1
B12-O12-Co2	26	0	50	104	154	H9-B2-O17-Co8	36	0	8	30	38
B12-O26-Co8	46	1	10	217	228	H9-B4-O15-Co8	36	0	19	125	144
B12-O36-Co10	58	0	0	1	1	H9-B5-O14-Co8	36	0	8	28	36
B16-Co8	24	0	4	11	15	H9-B6-O13-Co8	36	0	5	14	19
B16-O28-Co4	48	0	45	321	366	H10-O15-Co8	33	0	250	575	825
B16-O32-Co8	56	0	8	53	61	H10-B1-O14-Co8	33	0	9	217	226
B20-Co4	24	0	18	118	136	H10-B1-O15-Co7	33	0	1	8	9
B21-Co3	24	0	5	40	45	H10-B2-O13-Co8	33	0	47	155	202
B32-O56-Co8	96	0	3	188	191	H10-B2-O15-Co6	33	0	11	65	76
B64-Co32	96	0	2	0	2	H10-B3-O12-Co8	33	0	1	31	32
B80-Co16	96	0	28	68	96	H10-B3-O15-Co5	33	0	20	17	37
B84-Co12	96	0	8	4	12	H10-B4-O11-Co8	33	0	16	28	44
H1	1	0	1	0	1	H10-B5-O10-Co8	33	0	36	69	105
H1-Co16	17	0	134	1	135	H10-B7-O8-Co8	33	0	2	1	3
H1-Co26	27	0	41	0	41	H12-O17-Co8	37	0	197	445	642

H1-O1	2	0	3	0	3	H12-O18-Co8	38	0	39	0	39
H1-O1-Co15	17	0	21	0	21	H12-O22-Co16	50	0	0	10	10
H1-O2-Co30	33	0	55	0	55	H12-B1-O15-Co8	36	0	12	335	347
H1-O5-Co29	35	0	52	0	52	H12-B1-O16-Co8	37	0	35	259	294
H1-O6-Co31	38	0	49	0	49	H12-B1-O17-Co7	37	0	17	179	196
H1-O7-Co31	39	0	60	0	60	H12-B2-O15-Co8	37	0	18	130	148
H1-O7-Co32	40	0	19	0	19	H12-B2-O16-Co8	38	0	23	43	66
H1-O11-Co8	20	0	2	96	98	H12-B3-O14-Co8	37	0	51	145	196
H1-O14-Co15	30	0	6	2	8	H12-B3-O15-Co8	38	0	20	28	48
H1-O19-Co16	36	0	4	8	12	H12-B3-O17-Co5	37	0	0	1	1
H1-B1-O10-Co8	20	0	0	5	5	H12-B4-O13-Co8	37	0	28	142	170
H1-B1-O11-Co7	20	0	0	3	3	H12-B5-O12-Co8	37	0	10	38	48
H1-B2-O11-Co6	20	0	0	1	1	H12-B48-O92-Co14	166	0	0	106	106
H2	2	4	0	0	4	H13-Co19	32	0	0	1	1
H2-Co15	17	0	115	0	115	H13-B1-O16-Co8	38	0	115	1630	1745
H2-Co19	21	0	47	68	115	H13-B2-O14-Co8	37	0	6	59	65
H2-Co20	22	0	0	28	28	H14-Co20	34	0	2	45	47
H2-O2-Co1	5	0	0	6	6	H14-O7	21	0	1	759	760
H2-O2-Co16	20	0	0	20	20	H14-O13-Co4	31	0	11	12	23
H2-O2-Co29	33	0	66	0	66	H14-O16-Co8	38	0	96	239	335
H2-O2-Co30	34	0	17	0	17	H14-O17-Co8	39	0	80	229	309
H2-O3-Co28	33	0	44	0	44	H14-O19-Co8	41	0	130	240	370
H2-O4-Co2	8	0	0	6	6	H14-O30-Co16	60	0	0	8	8
H2-O10-	20	0	5	131	136	H14-B1-O15-	38	0	17	117	134

Co8						Co8					
H2-O11-Co8	21	0	7	277	284	H14-B1-O16-Co7	38	0	0	13	13
H2-O12-Co8	22	0	7	359	366	H14-B1-O16-Co8	39	0	7	79	86
H2-O14-Co14	30	0	6	0	6	H14-B1-O17-Co7	39	0	4	28	32
H2-O18-Co11	31	0	2	0	2	H14-B1-O18-Co8	41	0	8	133	141
H2-O18-Co12	32	0	4	0	4	H14-B1-O19-Co7	41	0	3	6	9
H2-O22-Co16	40	0	6	3	9	H14-B2-O14-Co8	38	0	2	10	12
H2-O30-Co24	56	0	4	7	11	H14-B2-O17-Co6	39	0	4	37	41
H2-B1-O9-Co8	20	0	0	2	2	H14-B2-O17-Co8	41	0	30	198	228
H2-B1-O10-Co8	21	0	1	50	51	H14-B3-O16-Co5	38	0	5	24	29
H2-B1-O11-Co7	21	0	12	106	118	H14-B3-O16-Co8	41	0	18	53	71
H2-B1-O11-Co8	22	0	5	180	185	H14-B4-O15-Co8	41	0	32	26	58
H2-B1-O12-Co7	22	0	3	158	161	H14-B5-O11-Co8	38	0	18	6	24
H2-B2-O8-Co8	20	0	1	7	8	H14-B5-O12-Co8	39	0	89	97	186
H2-B2-O9-Co8	21	0	2	26	28	H14-B5-O14-Co8	41	0	0	10	10
H2-B2-O10-Co8	22	0	16	280	296	H14-B6-O10-Co8	38	0	5	13	18
H2-B2-O12-Co6	22	0	2	23	25	H14-B6-O11-Co8	39	0	10	19	29
H2-B2-O20-Co16	40	0	0	77	77	H14-B8-O9-Co8	39	0	10	11	21
H2-B2-O22-Co14	40	0	0	72	72	H15-B1-O16-Co7	39	0	17	212	229
H2-B3-O9-Co8	22	0	15	118	133	H16-O8	24	0	14	3916	3930
H2-B4-O7-Co8	21	0	21	56	77	H16-O16-Co8	40	0	300	654	954
H2-B4-	22	0	4	36	40	H16-O32-Co16	64	0	3	21	24

O8-Co8											
H2-B4-O11-Co4	21	0	3	52	55	H16-B1-O15-Co8	40	0	328	822	1150
H3-O1-Co17	21	0	192	0	192	H16-B2-O14-Co8	40	0	201	302	503
H3-O2-Co28	33	0	0	54	54	H16-B2-O24-Co8	50	0	4	28	32
H3-O2-Co29	34	0	0	30	30	H16-B2-O32-Co14	64	0	1	157	158
H3-O3-Co27	33	0	44	0	44	H16-B3-O13-Co8	40	0	24	56	80
H3-O5-Co27	35	0	169	0	169	H16-B4-O44-Co32	96	0	0	15	15
H3-O6-Co3	12	0	4	1	5	H18-O38-Co16	72	0	1	6	7
H3-O14-Co14	31	0	11	0	11	H20-O30-Co16	66	0	0	11	11
H3-O21-Co14	38	0	2	0	2	H20-O34-Co16	70	0	15	31	46
H3-O21-Co15	39	0	17	0	17	H24-O32-Co16	72	0	8	0	8
H3-O21-Co16	40	0	5	18	23	H24-O34-Co16	74	0	0	13	13
H3-O96-Co63	162	0	0	1	1	H24-B4-O40-Co32	100	0	7	13	20
H3-B1-O21-Co15	40	0	5	49	54	H24-B8-O36-Co32	100	0	1	10	11
H4-O4-Co2	10	0	0	4	4	H24-B24-O20-Co32	100	0	9	18	27
H4-O6-Co28	38	0	173	0	173	H28-O32-Co16	76	0	19	7	26
H4-O8-Co4	16	0	111	93	204	H28-O34-Co16	78	0	0	5	5
H4-O12-Co8	24	0	34	303	337	H28-O38-Co16	82	0	1	3	4
H4-O18-Co9	31	0	35	0	35	H28-B2-O32-Co14	76	0	1	19	20
H4-O20-Co15	39	0	3	0	3	H28-B2-O38-Co14	82	0	15	7	22
H4-O20-Co16	40	0	23	9	32	H28-B4-O38-Co12	82	0	20	30	50
H4-O22-Co16	42	0	0	1	1	H28-B4-O56-Co32	120	0	12	37	49

H4-O23-Co14	41	0	1	0	1	H28-B4-O60-Co28	120	0	11	0	11
H4-O23-Co15	42	0	6	0	6	H28-B6-O32-Co16	82	0	1	32	33
H4-O23-Co16	43	0	3	4	7	H28-B8-O30-Co16	82	0	26	6	32
H4-O24-Co16	44	0	0	6	6	H28-B8-O52-Co32	120	0	1	10	11
H4-O30-Co22	56	0	7	0	7	H28-B12-O48-Co32	120	0	6	14	20
H4-O32-Co20	56	0	0	1	1	H28-B16-O44-Co32	120	0	4	28	32
H4-O128-Co84	216	0	0	2	2	H30-O15	45	124	4	94	222
H4-B1-O11-Co8	24	0	9	128	137	H32-O30-Co16	78	0	43	0	43
H4-B1-O12-Co7	24	0	3	58	61	H32-O32-Co14	78	0	31	0	31
H4-B2-O4-Co28	38	0	5	0	5	H32-O32-Co16	80	0	26	0	26
H4-B2-O10-Co8	24	0	7	38	45	H36-B16-O60-Co32	144	0	4	18	22
H4-B2-O16-Co9	31	0	11	49	60	H40-B4-O56-Co32	132	0	2	21	23
H4-B2-O18-Co16	40	0	0	21	21	H40-B4-O60-Co28	132	0	3	46	49
H4-B3-O9-Co8	24	0	8	48	56	H40-B8-O60-Co24	132	0	0	26	26
H4-B3-O15-Co9	31	0	4	10	14	H40-B16-O44-Co32	132	0	12	8	20
H4-B3-O17-Co16	40	0	9	67	76	H48-B4-O64-Co32	148	0	0	104	104
H4-B4-O8-Co8	24	0	3	18	21	H48-B4-O68-Co28	148	0	0	6	6
H4-B4-O12-Co4	24	0	2	18	20	H48-B8-O60-Co32	148	0	2	6	8
H4-B4-O16-Co16	40	0	1	27	28	H48-B8-O68-Co24	148	0	50	75	125
H4-B4-O44-	80	0	6	128	134	H48-B12-O56-Co32	148	0	2	24	26

Co28											
H4-B11-O13-Co16	44	0	6	8	14	H48-B16-O52-Co32	148	0	7	26	33
H4-B40-Co16	60	0	4	0	4	H48-B20-O48-Co32	148	0	1	8	9
H4-B44-O80-Co12	140	0	0	66	66	H52-O44-Co12	108	0	18	0	18
H5-Co22	27	0	144	0	144	H52-O45-Co12	109	0	23	0	23
H5-O2-Co26	33	0	164	72	236	H52-O46-Co12	110	0	13	0	13
H5-O2-Co27	34	0	0	36	36	H52-B9-O36-Co12	109	0	25	1	26
H5-O3-Co25	33	0	466	0	466	H52-B11-O35-Co12	110	0	8	0	8
H5-O4-Co24	33	0	158	0	158	H56-B4-O60-Co32	152	0	2	29	31
H5-O15-Co9	29	0	9	0	9	H56-B4-O64-Co28	152	0	14	116	130
H5-O19-Co16	40	0	7	13	20	H56-B4-O64-Co32	156	0	9	77	86
H5-O21-Co15	41	0	9	0	9	H56-B8-O68-Co24	156	0	29	156	185
H5-O21-Co16	42	0	5	10	15	H56-B24-O40-Co32	152	0	28	8	36
H5-B1-O2-Co25	33	0	11	0	11	H64-B4-O60-Co28	156	0	7	0	7
H5-B1-O16-Co8	30	0	0	114	114	H104-O32-Co4	140	0	18	68	86
H5-B2-O3-Co23	33	0	5	0	5	total	--	688	8847	32599	42134

Table S3. Benchmark of G-NN against DFT calculations for key structures of the Co-B-O-H composite system.

Chem. formula				N_{atom}	E_{DFT}(eV)	E_{NN}(eV)	E_{diff} (meV)/atom
Co	B	O	H				
					Bulk		
8	2	16	2	28	-175.232	-175.115	4.155
8	2	16	2	28	-174.673	-174.437	8.436
8	2	16	2	28	-174.937	-175.019	-2.929
8	0	16	8	32	-182.904	-182.921	-0.527
16	5	32	1	54	-344.913	-345.746	-15.422
24	8	48	0	80	-515.778	-514.798	12.248
16	1	32	13	62	-360.308	-359.923	6.224
					Slab		
32	64	12	16	124	-751.307	-751.071	1.905
32	64	12	15	123	-746.36	-746.311	0.393
32	64	12	14	122	-741.155	-740.953	1.655
32	64	12	13	121	-734.482	-734.967	-4.008
32	64	13	14	123	-744.524	-744.427	0.791

Table S4. Asummary of overpotential, tafel, BET, C_{dl} values of Co_xFe_y-B sample.

Cataltst	Overpvtential (mV)	Tafel (mV/dec)	BET (m^2/g)	C_{dl} (mF/cm^2)
Co-B	379	78.08	233	4.12
Co_9Fe-B	331	51.21	261	12.70
Co_4Fe-B	279	43.65	347	24.20
Co_7Fe_3-B	309	55.05	266	14.93
CoFe-B	335	54.97	259	9.45
Co-p	394	83.93	229	3.64
Co_4Fe	297	46.46	304	19.81

Table S5. Transmission EXAFS fitting parameters for Co_4Fe-B sample.

Shell	CN	R(Å)	σ^2(Å^2)	ΔE_0(eV)	R factor
Co-O	3.0±0.6	1.95±0.03	0.0030	0.1±5.3	0.0118
Co-O	2.6±0.6	2.11±0.03			
Co-Co/Fe	8.7±0.7	2.95±0.01	0.0102	-1.9±1.4	
Co-Co/Fe	9.3±1.1	3.48±0.01			
Fe-O	5.5±0.9	1.95±0.02	0.0127	-5.4±3.6	0.0071
Fe-O	0.5±0.1	2.03±0.02			
Fe-Fe/Co	4.9±0.3	2.98±0.01	0.0101	-2.6±1.6	
Fe-Fe/Co	5.0±0.5	3.48±0.01			

Reference

1 Z. Wu, X. F. Lu, S. Zang and X. W. (David) Lou, *Adv. Funct. Mater.*, 2020, **30**, 1910274.

2 I. S. Filimonenkov, G. A. Tsirlina and E. R. Savinova, *Electrochimica Acta*, 2019, **319**, 227–236.

3 Y. Pan, H. Ren, R. Chen, Y. Wu and D. Chu, *Chem. Eng. J.*, 2020, **398**, 125660.

4 X. Wang, L. Yu, B. Y. Guan, S. Song and X. W. (David) Lou, *Adv. Mater.*, 2018, **30**, 1801211.

5 J. Li, Y. Kang, D. Liu, Z. Lei and P. Liu, *ACS Appl. Mater. Interfaces*, 2020, **12**, 5717–5729.

6 R.-Q. Li, P. Hu, M. Miao, Y. Li, X.-F. Jiang, Q. Wu, Z. Meng, Z. Hu, Y. Bando and X.-B. Wang, *J. Mater. Chem. A*, 2018, **6**, 24767–24772.

7 R. Jin, J. Huang, G. Chen, W. Chen, B. Ouyang, D. Chen, E. Kan, H. Zhu, C. Li, D. Yang and K. (Ken) Ostrikov, *Chem. Eng. J.*, 2020, **402**, 126257.

8 K. Lan, J. Li, Y. Zhu, L. Gong, F. Li, P. Jiang, F. Niu and R. Li, *J. Colloid Interface Sci.*, 2019, **539**, 646–653.

9 Y. Tong, Q. Sun, P. Chen, L. Chen, Z. Fei and P. J. Dyson, *ChemSusChem*, 2020, **13**, 5112–5118.

10 Y. Chen, S. Ji, Y. Wang, J. Dong, W. Chen, Z. Li, R. Shen, L. Zheng, Z. Zhuang, D. Wang and Y. Li, *Angew. Chem. Int. Ed.*, 2017, **56**, 6937–6941.

11 X. Han, C. Yu, S. Zhou, C. Zhao, H. Huang, J. Yang, Z. Liu, J. Zhao and J. Qiu, *Adv. Energy Mater.*, 2017, **7**, 1602148.

12 B. T. Jebaslinhepzybai, T. Partheeban, D. S. Gavali, R. Thapa and M. Sasidharan, *Int. J. Hydrog. Energy*, 2021, **46**, 21924–21938.

13 P. Guo, J. Wu, X.-B. Li, J. Luo, W.-M. Lau, H. Liu, X.-L. Sun and L.-M. Liu, *Nano Energy*, 2018, **47**, 96–104.

14 L. Wu, D. Shi, S. Yan, W. Qiao, W. Zhong and Y. Du, *Int. J. Hydrog. Energy*, 2021, **46**, 2086–2094.

15 J. Cheng, X. Yue, C. Chen, X. Shen, S. Zeng, Z. Ji, A. Yuan and G. Zhu, *SSRN Electron. J.*, DOI:10.2139/ssrn.3902687.

16 G. A. Gebreslase, M. V. Martínez-Huerta, D. Sebastián and M. J. Lázaro, *J. Colloid Interface Sci.*, 2022, **625**, 70–82.

17 F. Diao, M. Rykær Kraglund, H. Cao, X. Yan, P. Liu, C. Engelbrekt and X. Xiao, *J. Energy Chem.*, 2023, **78**, 476–486.

18 J.-H. Oh, Y. H. Lee, M. Kim, S.-H. Hong, T.-H. Kim and S. Choi, *J. Environ. Chem. Eng.*, 2023, **11**, 109578.

19 M. A. Suliman, M. H. Suliman, A. Adam, C. Basheer, Z. H. Yamani and M. Qamar, *Mater. Lett.*, 2020, **268**, 127593.

20 R. K. Tripathy, A. K. Samantara and J. N. Behera, *Dalton Trans.*, 2022, **51**, 2782–2788.

21 X. Zhao, B. Wen, Q. Dong, P. Wang and X. Lyu, *Int. J. Hydrog. Energy*, 2025, **105**, 556–564.